



# Occultation-based Size and Shape of (269) Justitia

Marc W. Buie<sup>1</sup> , Hoor AlMazmi<sup>2</sup> (حور المازمي) , Paul Hayne<sup>3</sup> , Anna Marciniak<sup>4</sup> , Brian A. Keeney<sup>1</sup> ,  
 Fahad Alawadhi<sup>3</sup> (فهد العوضي) , Alia Almansoori<sup>3</sup> (علياء المنصوري) , Noora Rashed Alsaeed<sup>2</sup> ,  
 Amer Sarhan Alsawwafi<sup>5</sup> (عامر سرحان الصوافي) , Arvind Jayashankara Aradhya<sup>3</sup> , Dahlia Baker<sup>3</sup> , Samuel F. A. Cartwright<sup>3</sup> ,  
 Elad David<sup>6</sup>, Hugh M. Davidson<sup>7</sup> , Ian Faber<sup>3</sup>, Chelsea Ferrell<sup>8</sup> , William Goodwyn Ferrell<sup>8</sup>, Kai Getrost<sup>9</sup> ,  
 Julian Hammerl<sup>3</sup> , Parker Hinton<sup>3</sup> , Jack L. Jewell<sup>8</sup> , Roxanne L. Kamin<sup>9</sup>, John Keller<sup>3</sup> , Mykal Lefevre<sup>3</sup>, Steve Messner<sup>9</sup>,  
 Vadim Nikitin<sup>9</sup> , Heshani Pieris<sup>3</sup> , Arunima Prakash<sup>3</sup> , Julien Salmon<sup>1</sup> , Abdullah Essa Sharif<sup>2,3,10</sup>, Michael Skrutskie<sup>11</sup> ,  
 Kya C. Sorli<sup>3</sup> , Thibaud Teil<sup>3</sup> (تيبو تيل) , Anne J. Verbiscer<sup>11</sup> , and Jacopo Villa<sup>3</sup>

<sup>1</sup> Southwest Research Institute, 1301 Walnut St., Suite 400, Boulder, CO 80302, USA; [buie@boulder.swri.edu](mailto:buie@boulder.swri.edu)

<sup>2</sup> UAE Space Agency, Abu Dhabi, United Arab Emirates

<sup>3</sup> University of Colorado Boulder, 2000 Colorado Ave., Boulder, CO 80309, USA

<sup>4</sup> Astronomical Observatory Institute, Faculty of Physics, Adam Mickiewicz University, Słoneczna 36, 60-286 Poznań, Poland

<sup>5</sup> United Arab Emirates University, Al Ain, Abu Dhabi, United Arab Emirates

<sup>6</sup> Weizmann Institute of Science, Rehovot, Israel

<sup>7</sup> Denver Astronomical Society, P.O. Box 102738, Denver, CO 80250, USA

<sup>8</sup> Unaffiliated

<sup>9</sup> International Occultation Timing Association, USA

<sup>10</sup> Yahsat, Abu Dhabi, United Arab Emirates

<sup>11</sup> Department of Astronomy, University of Virginia, P.O. Box 400325, Charlottesville, VA 22904, USA

Received 2024 June 19; revised 2025 January 28; accepted 2025 January 29; published 2025 March 18

## Abstract

We present results from an occultation of a star by the asteroid (269) Justitia on 2023 August 31 UT using a deployment of 34 stations. Of the deployed stations, 29 were successful in collecting useful data and 19 recorded a positive occultation event. All stations were regularly spaced 2.45 km apart in the cross-track direction to cover  $\pm 3\sigma$  of the ephemeris uncertainty with a planning diameter of 59 km. We find that the shape of Justitia is irregular, with large-scale facets and a circular-equivalent radius in the range of 28.5–28.9 km. The inferred albedo is  $p_V = 0.072 \pm 0.007$  using a rotation-corrected absolute magnitude of  $H_V = 9.72$ . Astrometry from the occultation is provided.

*Unified Astronomy Thesaurus concepts:* Asteroid occultation (71); Main belt asteroids (2036); Astrometry (80); Albedo (2321)

*Materials only available in the [online version of record](#): data behind figure, machine-readable table*

## 1. Introduction

The Emirates Mission to the Asteroid Belt (EMA) is under development for a seven-asteroid tour of the main asteroid belt. (269) Justitia is planned to be the largest asteroid of the tour as well as the final rendezvous target of the mission (H. A. AlMazmi et al. 2024). Target characterization work for the Lucy Mission shows that ground-based occultation observations (e.g., M. W. Buie et al. 2021) can contribute to mission planning and encounter targeting, and we are beginning these support efforts for the EMA mission. Furthermore, the shape and size of an asteroid refined by occultation data can lead to improvement in the estimated albedo, and can be compared to the shape and size independently derived from photometry and lightcurves at visible and infrared wavelengths (A. Marciniak et al. 2019).

Justitia is a dark, spectrally red carbonaceous asteroid located in the middle main belt with a semimajor axis of 2.62 au, diameter  $\sim 50$  km, rotation period 33.13 hr, and geometric albedo  $0.061 \pm 0.007$  (A. K. Mainzer et al. 2019). Using the spectral slope at visible wavelengths, Justitia has been classified as a D-type asteroid in the Bus-DeMeo spectral classification scheme, or alternatively as an Ld-type asteroid

using the SMASSII system (S. J. Bus & R. P. Binzel 2002). However, more recent observations of its extreme near-infrared spectral slope led to the proposal that Justitia, along with (203) Pompeja, may be a volatile- and organic-rich body which originates from the Kuiper Belt (S. Hasegawa et al. 2021; O. A. Humes et al. 2024). More recent work by M. Mahlke et al. (2022) presents a new classification based on a larger data set in which a new Z type is proposed that includes Justitia. From this work, the Z-type objects represent 1.1% of their sample (23 asteroids) and appear to be distinct from D-type objects. Many of these newly classified objects were previously considered to be D type, and they suggest that perhaps the D and Z types are not fully disentangled, perhaps due to effects of space weathering. This recent work suggests Justitia is an unusual, but not unique, body in the asteroid belt.

This work presents a targeted effort to better characterize the principle science target for the EMA mission through the use of occultation observations. The primary goal was the determination of an accurate absolute size that would provide an improved value of the surface reflectivity. We report on a single observing campaign and the resulting data for Justitia.

## 2. Prediction

The target star used for the prediction (Gaia ID = 39346646372596224) was reasonably bright at  $G = 13.9$  and was identified from the Gaia Data Release 3 (DR3) catalog



Original content from this work may be used under the terms of the [Creative Commons Attribution 4.0 licence](#). Any further distribution of this work must maintain attribution to the author(s) and the title of the work, journal citation and DOI.

(Gaia Collaboration et al. 2021). The catalog star position from DR3 is (04:01:07.908171, +15:02:32.03519). The position at the epoch of the event is (04:01:07.908268, +15:02:32.05640), which includes corrections for proper motion and parallax with a propagated uncertainty of (0.161, 0.093) mas corresponding to (297, 172) m. This uncertainty is low enough that it was ignored for both the prediction and the data reductions that follow.

The expected apparent brightness of Justitia at the time of the occultation was  $V = 15.1$  using the absolute magnitude from the Minor Planet Center. The orbit estimate for Justitia was more than adequate for planning the occultation, with a 134 yr astrometric record. We used the orbit from the JPL Horizons ephemeris system for the position. The covariance from Horizons was projected onto the apparent path of Justitia and decomposed into a cross-track uncertainty of 3.7 km and down-track uncertainty of 1.2 s. Both quantities are given here as  $1\sigma$  values. The geocentric shadow speed was  $11.1 \text{ km s}^{-1}$  and the sky-plane scale at the object was  $1846 \text{ km arcsec}^{-1}$ .

The radiometric size estimate was a diameter of  $50.7 \pm 0.2$  from A. K. Mainzer et al. (2019). However, much larger estimates were also available in the literature:  $64.92 \pm 0.590 \text{ km}$  (J. R. Masiero et al. 2012), along with  $60.94 \pm 13.950 \text{ km}$  (J. R. Masiero et al. 2020), suggesting a higher upper bound for the diameter. The absolute magnitude from the Minor Planet Center database was  $H_V = 9.78$  with no uncertainty provided. Using  $3\sigma$  bounds of these diameter measurements gives a diameter range from 50.1 to 66.7 km and implies a range of geometric albedo from 0.05 to 0.09. Adding a notional 0.1 mag uncertainty to  $H_V$  expands the albedo range to 0.1–0.045. The implied albedos did not provide additional constraints on size.

Our newly developed preliminary thermophysical model using new lightcurve-based shape models suggested a narrower range of sizes: 56–59 km. These shape models (which include the mirror-pole ambiguity), predicted a cross-track projected size of 59 km for the rotational phase at the time of the occultation (for details, see the companion paper by A. Marciniak et al. 2025). The thermophysical model used for planning was based on a simultaneous inversion of dense lightcurves in the visible range, and combined mid-infrared data from various satellites, in a convex inversion thermophysical model (CITPM) method developed by J. Ďurech et al. (2017). At this stage, two mirror-pole models still existed, with two symmetric shape solutions, both for a retrograde sense of rotation and differing in spin axis longitudes by  $180^\circ$ , but this ambiguity was expected to be resolved by the upcoming occultation.

For the purposes of planning for this occultation, the relevant size was the maximum reasonable size, which determines the expected size of the asteroid's shadow and therefore the spread of the stations needed on the ground. We based our deployment strategy on the largest size permitted by our thermophysical model calculations. The final pre-event prediction is shown in Figure 1 for the gray shaded region bounded by dashed lines for a cross-track diameter of 59 km.

### 3. Deployment

The original goal for this deployment was to deploy 50 stations to obtain a high-density set of chords rather than just trying for a few chords to get a spherical or elliptical size estimate. With these data, we expected to provide information

that would resolve the mirror-pole ambiguity and improve upon previous diameter and albedo estimates.

In keeping with past large coordinated campaigns for the Lucy mission (M. W. Buie et al. 2021), a large fraction of the observers were new to occultations. We recruited from the EMA development team as well as students from the University of Colorado Boulder. A few veteran observers from previous Lucy campaigns were included to assist with training and other support during the campaign. Overall, the final team included 54 people, offering a combination of stations using a mixture of solo and multiple-person teams. Training was conducted with numerous sessions in the 6 weeks prior to the campaign. The deployment campaign itself was designed around two nights for additional training and practice followed by a dress rehearsal night and then the final night for the occultation itself. In the end, we were unable to deploy the desired 50-station array and had to adjust the deployment strategy for a 34-station deployment. The total spread of stations was set at 81 km for  $3\sigma$  coverage with the largest credible diameter for Justitia set to 59 km, leading to a final track spacing of 2.45 km.

A significant factor in the deployment planning was maintaining as much flexibility against bad weather conditions as we could practically manage. Everyone was expecting to leave from the Boulder, Colorado area and the closest place in the shadow path was in Wyoming. The weather is not certain to be clear in late August in Wyoming, so we carried options to deploy as far west as the northeast corner of California. The longer drive time for deployment meant that the final decision on location had to be made no later than 3 days before the event day. The weather pattern was very stable, and we made the decision to deploy to Wyoming 4 days prior to the event. The base of operations was in Wheatland, putting the deployment drive at about an hour for the site most distant from the base.

Nearly all of the equipment was from the collection of gear used for Lucy-related occultations. These systems use a Celestron CPC1100 (28 cm) telescope, which is the same as that used by RECON (M. W. Buie & J. M. Keller 2016). These systems are all outfitted with a HyperStar in place of the secondary mirror that permits working at prime focus. All systems have an electronic focuser, essential for the precise focus needed with this fast optical system ( $f/1.9$ ). The teams used QHY174M-GPS CMOS cameras, which provide accurate GPS timing and have been a key component of successful occultation campaigns since the first Arrokoth event in support of New Horizons (M. W. Buie et al. 2020). The cameras were configured with GAIN = 300, offset = 100, 16-bit data (actually 12-bit shifted by 4 bits to inhabit the most significant bits), and full-frame images all saved in FITS format using SharpCap version 4.0.9562.0. The total readout overhead for our 900-frame collection was 0.44 s, corresponding to an average readout time of 0.5 ms per image. This dead time is negligible for these observations and is ignored in our analysis. All observations were unfiltered for maximum throughput. Additional details on the equipment can be found in M. W. Buie et al. (2020) and M. W. Buie et al. (2021).

Each team was given a track at a fixed offset from the predicted center line, and the task of finding a location to observe from that was within  $\sim 120 \text{ m}$  of the line. The final locations chosen by the teams are shown in Figure 1. The gray region bounded by dashed lines shows the predicted track and object size used to guide the deployment.

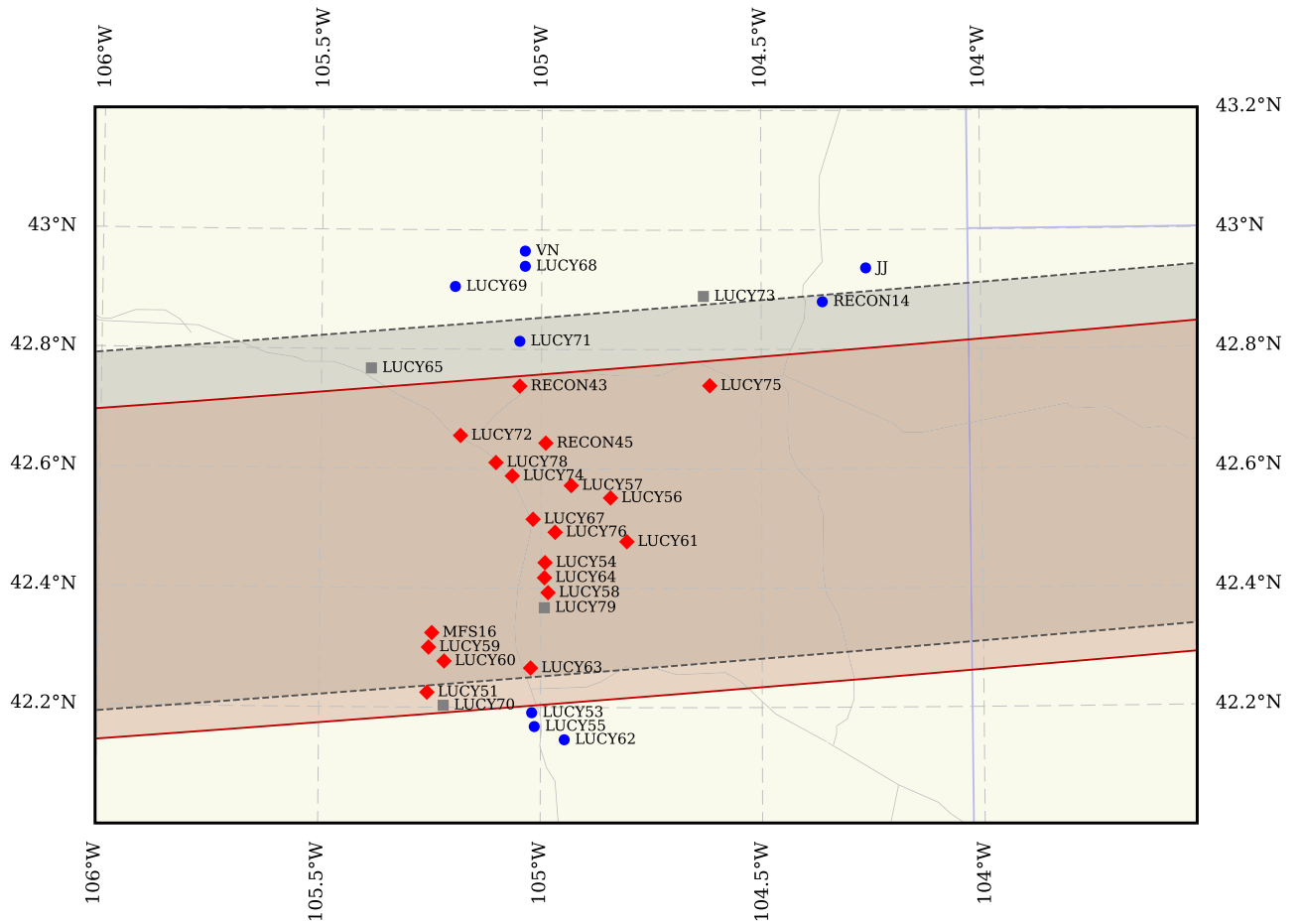


**Figure 1.** Deployment area for JU20230831. The prediction is denoted by the gray shaded area bounded by dashed lines for the anticipated 59 km diameter. The red shaded region bounded by the solid lines shows a 54.4 km-wide track that is consistent with the observations. The red diamonds denote sites with positive detections of an occultation. The blue circles indicate the locations of sites that had data ruling out an occultation. The gray squares are for deployed sites that were unable to collect useful data. Two sites (TM:failed and SM:negative) are not shown for clarity due to their distance from the main group.

The complete list of stations and teams is given in Table 1 along with their WGS84 positions, names of the observers, start and stop times of any data collected, their cross-track offset from the prediction, and relevant comments. The table is sorted by cross-track offset from north to south. The site names are derived from the internal designations for Lucy and RECON equipment and observer initials for privately owned equipment. The requested observing duration was 6 minutes, starting at 10:23:00 UT and ending at 10:29:00 UT, and most sites followed this instruction. This length of time was chosen to permit uniform instructions for the teams despite slight differences in the predicted mid-time while also providing some tolerance for individual inaccuracies in starting the data collection.

Two sites (TM and SM) are not shown on Figure 1 due to their large down-track offset relative to the main group. Those sites marked with gray squares deployed but were unable to collect constraining data. Blue circles denote sites that clearly show no signs of an occultation. Red diamonds indicate sites that recorded a definitive occultation. The red shaded region shows a 54.4 km shadow path that is manually adjusted from the ephemeris to be consistent with the observations. The exact edge is not known to better than the spacing at the limit, but the track shown here is made consistent with the inferred shape.

#### 4. Observations

Of the 34 deployed stations, 29 recorded useful data. Ten stations recorded data with no sign of an occultation. Data from 19 stations showed a clear occultation signature. The shortest chord (RECON43) had a duration of 1.030 s for a length of 11.2 km at Justitia. The longest chord (LUCY57) was 5.773 s (62.6 km).

The images collected were processed to extract a lightcurve of the target star and a nearby reference star. The reference star is used for a photometric reference to help remove any transparency variations. That star is also used as a tracking reference. The target star is measured as an offset from the reference star rather than for its absolute position. Any frame where a useful flux is detected on the target is used to build a fitted polynomial to the offset from the reference. The offset varies slightly during the observation due to field rotation.

Having a time-dependent offset prevents loss of positional lock on the target star during the occultation and ensures that the reappearance is accurately measured. This is a general procedure applied during our data analysis but was deemed unnecessary for this campaign since Justitia was detected during the occultation and the flux at the target star position never drops to zero.

**Table 1**  
Mobile Observing Stations and Teams for 2023 August 31

ID	UT Start	UT End	Lat. (deg)	Long. (deg)	Alt. (m)	Observers	Offset (km)	Comments
VN	10:22:57	10:29:02	42.964717	−105.037610	1483.1	Vadim Nikitin	40.66	
LUCY68	10:23:12	10:29:12	42.939238	−105.037516	1534.8	Vadim Nikitin	38.19	
LUCY69	10:22:59	10:28:59	42.904997	−105.196674	1516.4	Thibaud Teil, Dan Kubitschek	35.77	
JJ	10:23:00	10:29:04	42.935885	−104.261476	1349.2	Jack Jewell, Parker Hinton	33.28	
LUCY73	10:23:01	10:29:01	42.889002	−104.631581	1502.0	Reem Klaib, Salama Almazrouei, Fahad Albaeek	30.87	Bad image quality, wrong field.
RECON14	10:23:02	10:29:02	42.879534	−104.360607	1543.6	Kai Getrost	28.41	
LUCY71	10:22:57	10:28:57	42.813555	−105.049408	1609.0	Hunter Daboll, Mariam Alharmondi	25.98	
LUCY65	...	...	42.767624	−105.386757	1473.9	Alia AlMansoori, Fahad Alawadhi	23.45	Wrong field.
SM	10:25:20	10:29:20	43.204478	−093.081997	334.0	Steve Messner	21.05	
RECON43	10:23:01	10:29:01	42.738433	−105.048965	1528.3	Roxanne Kamin, Mykal Lefevre	18.58	
LUCY75	10:23:33	10:29:30	42.739347	−104.617325	1635.1	Safa AlHasani, Moza AlSerkal	16.18	
TM	...	...	41.316218	−120.115264	1412.8	Terry Miller	13.82	Equipment problems.
LUCY72	10:22:01	10:28:01	42.655376	−105.183333	1432.8	Abdullah Sharif, Khaled AlNagbii	11.19	
RECON45	10:23:01	10:29:01	42.643048	−104.989583	1485.2	Brian Keeney	8.84	
LUCY78	10:22:58	10:28:58	42.610281	−105.102630	1431.1	Hugh Davidson	6.27	
LUCY74	10:23:02	10:29:02	42.587901	−105.065507	1427.3	Ian Faber, Anna Sophia Rorrer Warren	3.85	
LUCY57	10:22:59	10:29:02	42.572063	−104.931730	1429.4	Chelsea Ferrell, Wyn Ferrell	1.50	
LUCY56	10:23:00	10:29:03	42.551412	−104.842626	1509.9	Anne Verbiscer	−1.02	
LUCY67	10:22:58	10:28:58	42.515422	−105.018012	1426.1	Amer Alsawwafi, Sultan Alblooshi	−3.56	
LUCY76	10:22:59	10:28:59	42.493737	−104.967979	1431.4	Jacopo Villa, Hamdan Almansoori	−5.98	
LUCY61	10:22:59	10:29:02	42.478079	−104.805457	1598.2	Julian Hammerl, Sean Fitze	−8.41	
LUCY54	10:23:02	10:29:02	42.442744	−104.990694	1438.0	John Keller	−10.85	
LUCY64	10:23:01	10:29:01	42.417481	−104.991818	1417.3	João Vaz Carneiro	−13.34	
LUCY58	10:22:58	10:29:02	42.392536	−104.983700	1417.9	Hoor AlMazmi, Fatema AlHameli	−15.85	
LUCY79	...	...	42.367201	−104.991958	1462.8	Paul Hayne, CJ O'Neill	−18.27	Telescope GPS failed.
MFS16	10:23:01	10:29:01	42.324860	−105.246075	1778.1	Michael Skrutskie	−20.76	
LUCY59	10:23:01	10:29:01	42.300551	−105.253354	1744.4	Dahlia Baker, Heshani Pieris	−23.12	
LUCY60	10:23:01	10:29:02	42.277357	−105.218043	1676.5	Sam Cartwright, Elad David	−25.65	
LUCY63	10:22:58	10:28:59	42.266195	−105.022643	1505.9	Noora Alsaheed, Kya Sorli	−28.01	
LUCY51	10:23:01	10:29:02	42.224973	−105.256319	1713.4	Marc Buie	−30.56	
LUCY70	...	...	42.203159	−105.219410	1627.4	Tom Masterson	−32.98	Power glitch.
LUCY53	10:22:58	10:29:02	42.191230	−105.019891	1448.5	Brian Kirby, Elizabeth Gilje Kirby	−35.44	
LUCY55	10:22:59	10:29:02	42.168086	−105.013996	1405.2	Julien Salmon	−37.78	
LUCY62	10:23:02	10:29:02	42.146090	−104.946369	1374.3	Arvind Aradhva, Arunima Prakash	−40.36	

**Note.** All times are on 2023 August 31. All site locations are referenced to the WGS84 datum. Offset is the distance perpendicular to the center line of the last pre-event prediction.

At site LUCY51, data were taken at an air mass of 1.426 an hour before the occultation when Justitia and the star were clearly separated. Two hundred frames were collected with 1.0 s exposures. The individual fluxes were measured and the flux ratio (Justitia/star) in our instrumental system was determined to be  $0.534 \pm 0.005$  and used for all systems in the subsequent analysis. Changes in this value from system to system will be negligible due to the uniformity of equipment. We did not correct the baseline for the lightcurve of Justitia due to its long rotation period and its lightcurve amplitude. This latter correction would be at most 0.03 mag, below the level of the per-point noise in the occultation data, and would not affect the extracted timing values at a significant level.

Second-order extinction in the instrumental system was ignored in our analysis. The occultation data were taken at an air mass of 1.256. The ( $B_p - R_p$ ) color of the asteroid in the Gaia system is estimated to be 1.10, given a ( $g - r$ ) color of 0.75 from the Fink Portal. No significant color term is seen for this color and air-mass difference.

The extracted lightcurves are shown in Figures 2–4. Only 20 s are shown on either side of the predicted mid-time, but the entire data set collected is provided in the supplemental data

files. The legend on the right notes the site code, cross-track offset, predicted mid-time at the site, the standard deviation (with  $3\sigma$  outlier rejection) of the baseline flux, measured time between frames in seconds, and duration converted to down-track distance in kilometers. Uncertainties are omitted from the plots for clarity. All lightcurves are normalized to unity for the unocculted signal, which is the sum of Justitia and the target star fluxes. The mid-occultation baseline is  $0.347 \pm 0.002$ , which is the flux from Justitia and determined from the flux ratio described above. The occulted data from all systems is consistent with the measured flux ratio.

Some of the occulted data appear to have structure, but close inspection of the images reveals that structure to be a property of the noise during the occultation. This noise is caused by larger errors in the measured position, and the resulting measurement is driven by nonrandom elements in the background (e.g., hot pixels). No signs of a resolved stellar diameter are seen. All transitions are consistent with the moment of occultation falling during an integration. More discussion will follow regarding the data in the context of the derived limb profile (see Section 5).

No significant dropouts are seen in the data outside of the solid-body occultation region. Rings or satellites can be ruled



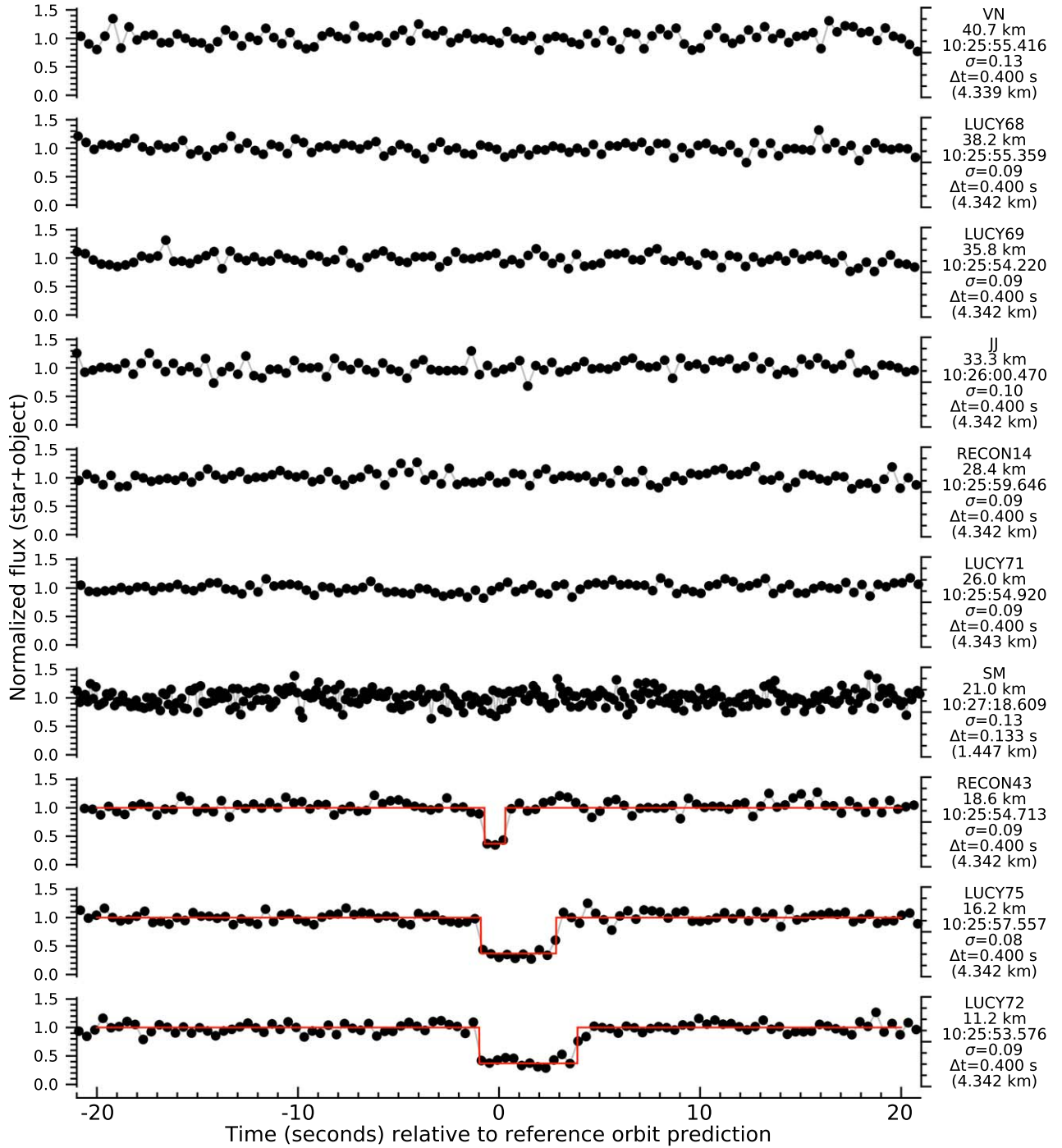


**Figure 2.** Lightcurve data for JU20230831, part 1. Normalized lightcurves are shown where unity is equal to the sum of the flux from the target star and Justitia. Each data set is labeled with the site ID, the cross-track offset, the predicted mid-time, the uncertainty per point ( $\sigma$ ), and the time and spatial resolution of the data. Complete lightcurves are provided for Figures 2–4 as data behind the figure.

(The data used to create this figure are available in the [online article](#).)

out in the region probed by our observations. No such features were expected, and rigorous quantitative limits are beyond the scope of the present study. If subsequent observations were to detect possible rings or satellites, our published data could then be reanalyzed as needed.

## 5. Results

For each lightcurve showing an occultation, we note the first and last point of the occultation. From this, we compute a

model lightcurve at very high time resolution that is then binned down to match the resolution and sampling of the actual data. Our model is a trivial approach where the star is either seen or not seen at any instant in time, and we have two fitted parameters corresponding to the time of disappearance and then the time of reappearance. The flux in the transitional point is used to determine the time of the edge and the photometric uncertainty derived from the unocculted baseline is used to compute the error in that time. This method always leads to an uncertainty smaller than the time resolution but is consistent

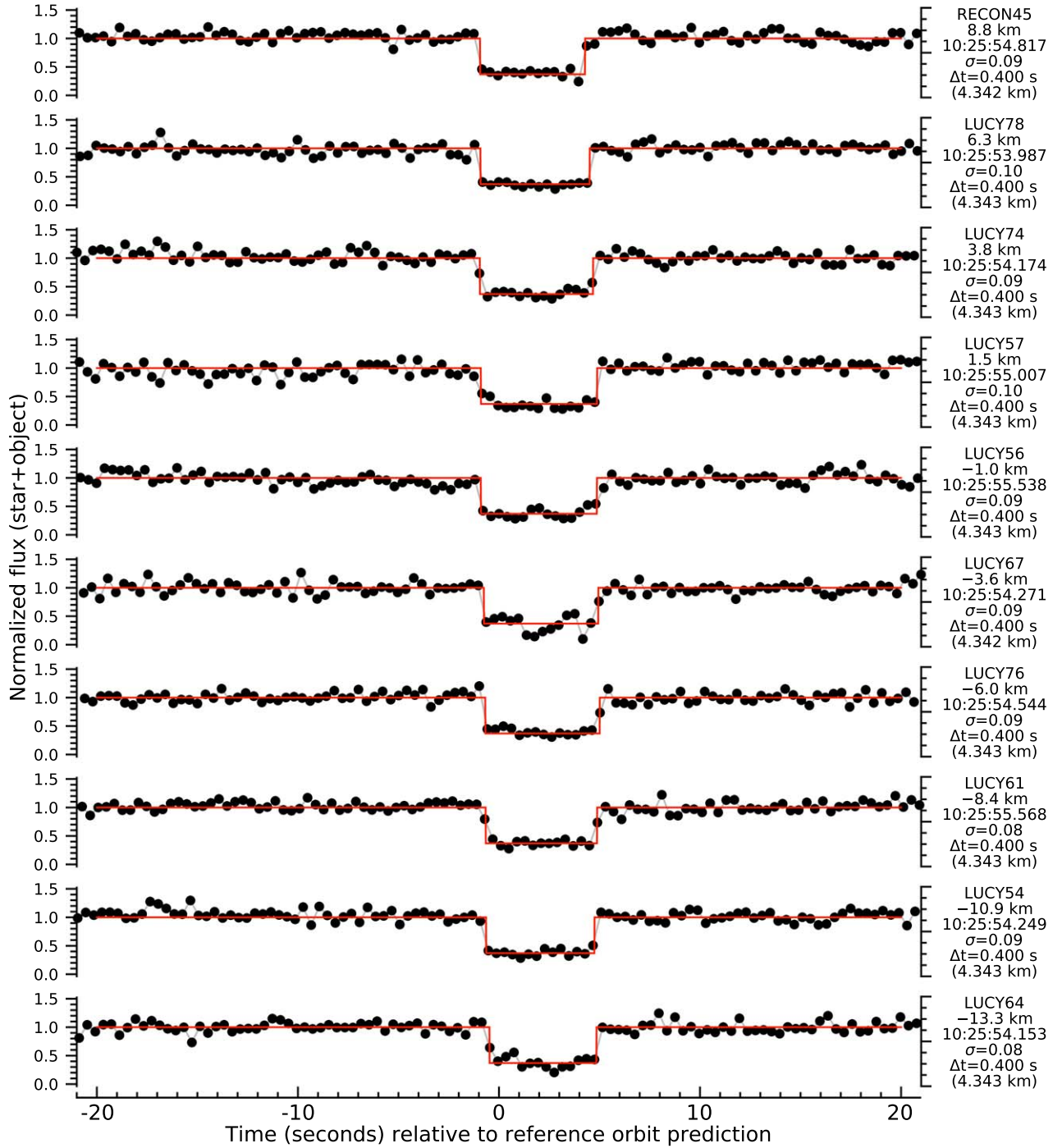


**Figure 3.** Lightcurve data for JU20230831, part 2. Normalized lightcurves are shown where unity is equal to the sum of the flux from the target star and Justitia. Each data set is labeled with the site ID, the cross-track offset, the predicted mid-time, the uncertainty per point ( $\sigma$ ), and the time and spatial resolution of the data.

with the noise level in the data. Our model ignores the effects of a resolved stellar disk or any diffraction effects since there is no evidence for either in the data.

Table 2 lists the time of disappearance (D) and reappearance (R) for each station. The uncertainty of the derived timing is also listed. Also tabulated are the tangent plane coordinates of the D and R events converted to kilometers based on the distance to the object at the time of the event for each observing site. This representation of the occultation edges removes all of the observer-based geometry and provides information in a plane containing the center of the object. Any shift seen for the

object center relative to the origin is an indication of the error in the ephemeris of the object, and precise astrometry can be derived from the occultation.

Figure 5 provides a graphical representation of the limb points from Table 2. The plane plotted here is the tangent plane defined by the occultation star that is then shifted by the ephemeris of the occulting body to remove the time and observing geometry information. The result is the shape of the object as seen in a frame comoving with the object. Each line on the plot depicts the motion of the star relative to Justitia as seen by each site. Each line is labeled with the ID tag of the

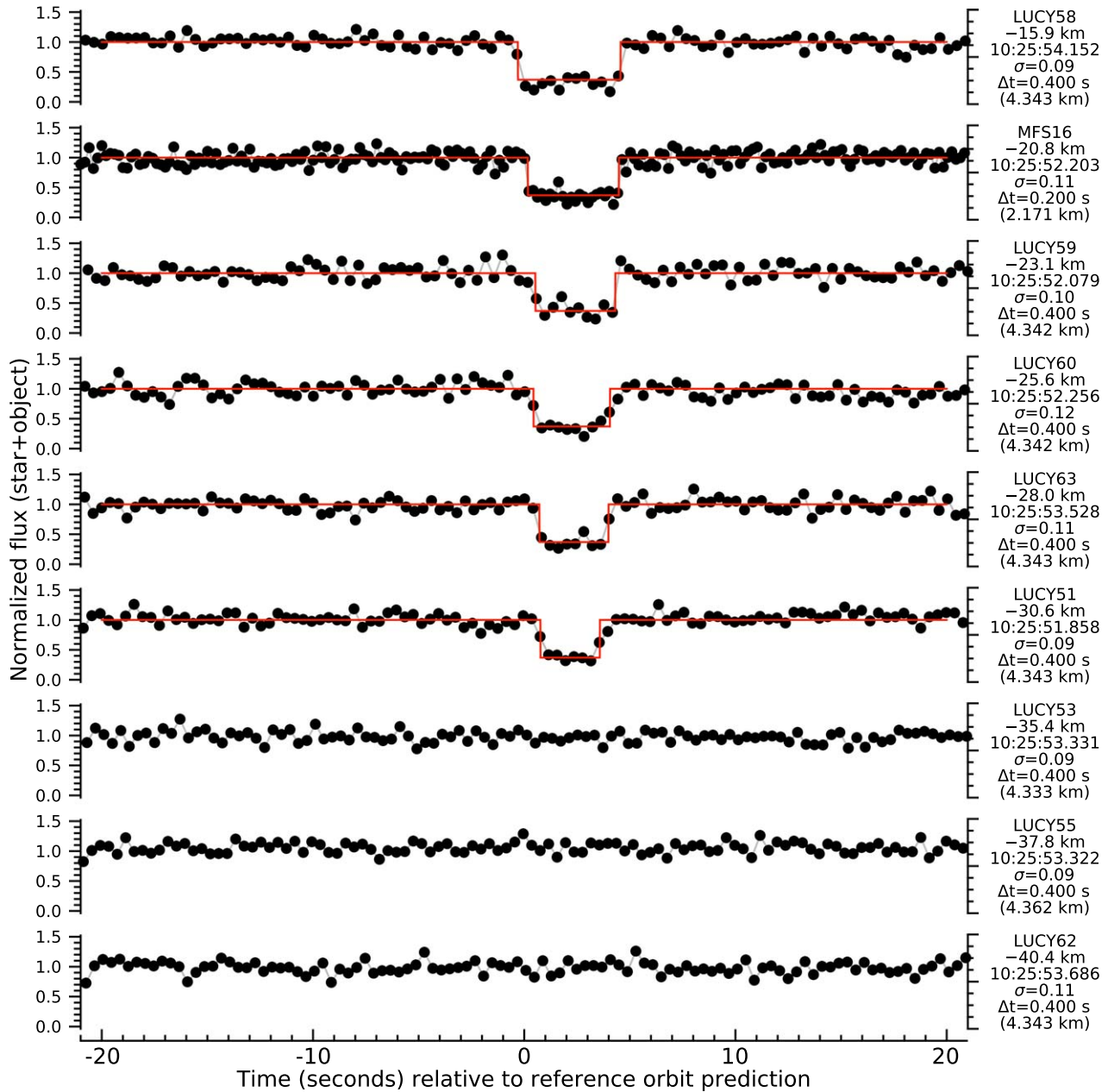


**Figure 4.** Lightcurve data for JU20230831, part 3. Normalized lightcurves are shown where unity is equal to the sum of the flux from the target star and Justitia. Each data set is labeled with the site ID, the cross-track offset, the predicted mid-time, the uncertainty per point ( $\sigma$ ), and the time and spatial resolution of the data.

station. The direction of apparent stellar motion is shown by the arrow in the upper-right corner. This coordinate system is in the J2000 system, and north ( $\eta$ ) and east ( $\xi$ ) are labeled.

Lines shown in faint gray are for stations that were unable to collect useful data and thus provide no constraint on the shape or position. The red lines indicate stations that clearly show no occultation was seen from their vantage point. The blue lines indicate those stations that recorded an occultation, and the orange points show the positions of the edges retrieved from the lightcurve data. The uncertainties are plotted but are all smaller than the orange symbols.

Two different representations of the projected limb of Justitia are shown. The cyan curve is an ellipse that is fitted to the limb points (unweighted). This fit does not incorporate any of the negative constraints provided by stations seeing no event, only the positive detections. Not only does the ellipse not track the

data very well, it also violates the negative constraint from station SM. The red diamond in the center is the formal center of the fitted ellipse.

The dark purple curve is a function-free representation of the limb. This curve does not represent a fit but rather a curve that is consistent with all the data subject to the constraints imposed by the curve generation algorithm. This curve is generated by converting the Cartesian coordinates to polar coordinates. The center used for this conversion is the mean of the extrema of  $\xi$  and  $\eta$ , but the actual value of this center is not critical. In polar coordinates, a locally weighted scatterplot smoother (LOWESS) curve is computed that follows the data points according to their uncertainties. This step requires setting a smoothing width that corresponds to the angular resolution of the curve. For this curve the angular smoothing width (triangular weighting profile) was set to  $20^\circ$ . This smoothing

**Table 2**  
Occultation Event Information for 2023 August 31

ID	Type	UT	$\sigma$ (s)	$\sigma$ (km)	$\xi$ (km)	$\eta$ (km)
LUCY51	D	10:25:52.625	0.035	0.39	-10.294	-29.972
LUCY51	R	10:25:55.438	0.035	0.39	-44.305	-27.821
LUCY54	D	10:25:53.613	0.038	0.42	6.179	-11.270
LUCY54	R	10:25:58.998	0.038	0.42	-52.100	-7.577
LUCY56	D	10:25:54.639	0.037	0.41	9.635	-1.634
LUCY56	R	10:26:00.407	0.036	0.40	-52.762	2.322
LUCY57	D	10:25:54.111	0.040	0.44	9.782	0.883
LUCY57	R	10:25:59.884	0.040	0.44	-52.688	4.843
LUCY58	D	10:25:53.852	0.034	0.38	2.245	-16.018
LUCY58	R	10:25:58.715	0.034	0.38	-50.372	-12.686
LUCY59	D	10:25:52.607	0.041	0.46	-7.095	-22.719
LUCY59	R	10:25:56.392	0.041	0.46	-48.055	-20.126
LUCY60	D	10:25:52.700	0.048	0.53	-6.433	-25.296
LUCY60	R	10:25:56.320	0.047	0.52	-45.592	-22.818
LUCY61	D	10:25:54.903	0.030	0.33	6.694	-8.849
LUCY61	R	10:26:00.445	0.030	0.33	-53.276	-5.049
LUCY63	D	10:25:54.249	0.043	0.48	-9.558	-27.459
LUCY63	R	10:25:57.521	0.042	0.47	-44.967	-25.216
LUCY64	D	10:25:53.680	0.033	0.37	4.451	-13.653
LUCY64	R	10:25:59.005	0.033	0.37	-53.203	-10.002
LUCY67	D	10:25:53.523	0.038	0.42	7.870	-4.059
LUCY67	R	10:25:59.215	0.038	0.42	-53.718	-0.156
LUCY72	D	10:25:52.593	0.036	0.40	11.400	10.485
LUCY72	R	10:25:57.476	0.036	0.40	-41.437	13.836
LUCY74	D	10:25:53.222	0.038	0.42	10.444	3.198
LUCY74	R	10:25:58.856	0.038	0.42	-50.519	7.059
LUCY75	D	10:25:56.657	0.034	0.38	10.775	15.526
LUCY75	R	10:26:00.394	0.034	0.38	-29.671	18.088
LUCY76	D	10:25:53.868	0.035	0.39	6.914	-6.431
LUCY76	R	10:25:59.550	0.035	0.39	-54.563	-2.536
LUCY78	D	10:25:53.063	0.041	0.46	10.371	5.631
LUCY78	R	10:25:58.499	0.041	0.46	-48.460	9.358
MFS16	D	10:25:52.377	0.022	0.24	-3.197	-20.598
MFS16	R	10:25:56.686	0.021	0.23	-49.820	-17.643
RECON43	D	10:25:53.994	0.036	0.40	8.863	18.050
RECON43	R	10:25:55.025	0.036	0.40	-2.315	18.759
RECON45	D	10:25:53.879	0.036	0.40	10.775	8.174
RECON45	R	10:25:59.102	0.034	0.38	-45.739	11.757

**Note.** All times are on 2023 August 31 UT. ( $\xi$ ,  $\eta$ ) positions are J2000 offsets in the tangent plane defined by the occultation star.

(This table is available in machine-readable form in the [online article](#).)

width is a compromise since it does not vary around the body. In some locations, this smoothing does little due to the larger angular step size near the cross-track limits of the data, roughly the top and bottom of the limb. In other locations, e.g., near points 37–5 and 9–13, the smoothing is partially averaging over real fine-scaled structure of the limb.

The shown hull in Figure 5 is further controlled by points 8 and 29–31 that prevent the curve from violating negative constraints. These extra constraints are manually chosen to produce a curve that looks reasonable, but those choices are not unique and no truly statistical measure can assess the differences as long as the negative constraints are not violated. At the core of this challenge there remains a fundamental truth: unseen topography cannot be constrained.

The area contained within the LOWESS curve is 2625 km<sup>2</sup> while the area of the fitted ellipse is 2762 km<sup>2</sup>. The circular equivalent size of Justitia at the time of the occultation is thus  $R = 28.9$  km (diameter of 57.8 km). This area represents a value close to the upper limit defined by the negative

observation at the LUCY53 site. Consider one possible alternate limb placement in this location. When we force the limb to miss LUCY70, as well, the area drops to 2557 km<sup>2</sup> and is close to the lower limit of the area. This alternate option suggests the circular equivalent radius could be smaller by 0.4 km.

For these data, there are extra control points (29–31) in between the reappearances from RECON43 and LUCY75. Without the control points, the automatically generated curve crosses LUCY75 an extra two times. Since the data do not show a double occultation, that curve is excluded. In this case, the range of permissible curves consistent with the data is tightly constrained, and what we do not know here will not change the inferred projected area or the center of body measurements by any meaningful amount.

An extra control point (8) was needed on the bottom of the curve. The lack of data from LUCY70 means the location of the edge is uncertain by two track spacings or 4.9 km. The choice made here was to create a smooth curve with the largest area



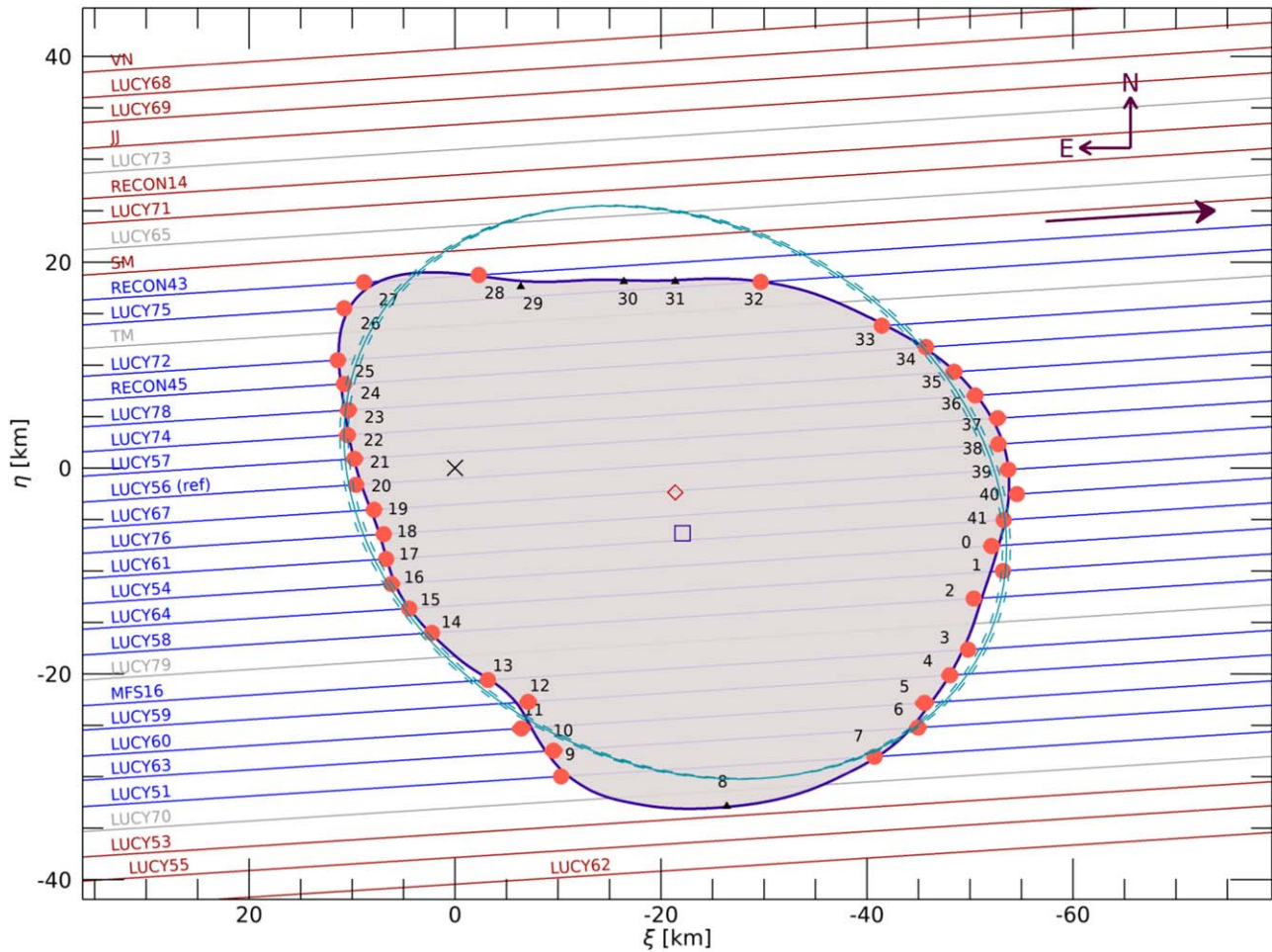


**Figure 5.** Limb profile for Justitia for the JU20230831 campaign. This diagram is shown in a sky-normal orientation (north and east are labeled). The origin (black X) denotes the ephemeris location of Justitia. Each line represents the path of the star relative to the object. Blue lines are for sites that recorded a positive occultation. Red lines are for sites that recorded data but did not see an occultation. Gray lines are for sites that were deployed but were unable to take any useful data. The direction of apparent motion of the star is given by the arrow in the upper-right corner of the plot. The orange dots show the location where the star either disappears or reappears. The cyan ellipse is the best-fitting ellipse to the limb points (unweighted) and the close dashed lines are fits to the systematic extremes given the uncertainties ( $-\sigma$  on the left and  $+\sigma$  on the right for the largest, reversed for the smallest). The solid limb curve is a function-free representation of a limb that is consistent with all of the data (see text for details). The red diamond shows the center of the fitted ellipse and the purple square is the center of the limb profile. Each point on this limb has a number to facilitate discussion, and extra control points are plotted small black triangles.

consistent with the data. The area could be as much as  $80 \text{ km}^2$  smaller, corresponding to an area 3% below the nominal value reported above and a change of 0.5 km in the circular equivalent size.

The combination of observed points on the limb and the extra control points defines the limb hull shown on Figure 5. The hollow square on the figure is the geometric mean position of this hull area.

There are some features in the lightcurves worthy of comment in light of the extracted limb profile even though all of these features are interpreted as noise in the end. The data from LUCY72 (point 33), RECON45 (point 34), LUCY56 (point 38), LUCY60 (point 6), and LUCY51 (point 7) all show a measurement just after reappearance that is slightly below the unocculted flux level (see Figures 2–4).

We are drawn to consider the two low points from LUCY72 and RECON45 as special due to being on adjacent chords at reappearance. Their placement along the limb precludes the interpretation of a correlated structure between the sites for the two apparently low points. An explanation based on the limb structure requires very small features in the horizontal direction

and relatively large features in the vertical direction (here horizontal and vertical are meant to refer to radial and tangential directions along the limb). The flux “drop” implies obscuring material along-track that is roughly 900 m wide somewhere during the low integration. This point of obscuration would fall at a point that is between 2 and 6 km above the surface as defined by the curve of the nearby reappearances. These dimensions seem unphysical. If both are related to real structures, they must be independent and the simpler explanation is a noise feature.

The resolution of the low points for the LUCY56 and LUCY60 data is more straightforward. For both of these tracks, the local slope would require the obscuring material to be detached from the body or follow a serpentine path starting from the body as seen on the plane of the sky to avoid detection by the other sites. These extra low points are interpreted as noise that is unrelated to the occultation.

The case for the LUCY51 data is more nuanced. In this case, the reappearance point (7) falls along a portion of the limb where the angle between the track and the limb is shallow. Under these circumstances, topographic features can more easily cause an extra short interruption of the starlight.

However, this extra feature must occur to the right of point 7 without affecting the position of the limb at point 6. This feature can be closer to point 7 than was the case for point 33, and the limb angle is slightly lower. As a consequence, the width is about the same and the height is slightly lower.

While the LUCY51 case is the strongest of the five, it is still does not seem to be very likely to be a real occultation signature. The more simple explanation is that all five of these represent the consequence of the noise in the lightcurves. Point 7 is only slightly more than  $1\sigma$  below the unocculted level. All of these five cases are similarly low, and for 19 lightcurves one would expect six measures greater than  $1\sigma$ . What makes this statistically odd is that these points appear more likely to be low rather than high, and the same statistical fluctuations are not obviously present either high or low at the disappearances. In lieu of a rigorous explanation, we thus proceeded with the assumption that these points do not record any extra occultation signatures.

The origin of Figure 5 corresponds to the position of star, and if the ephemeris were perfect, the center of Justitia would be at the origin. Most of the positional error in the ephemeris is along the direction of motion, which happens to also be close to the projected orbital motion of the asteroid. The inferred astrometric position of Justitia for this event is  $(\alpha, \delta) = (04:01:07.908248, +15:02:32.05278)$ . This position is for 2023 August 31 10:25:57.523 UTC for a topocentric position of N42.551412, W104.842626 at an elevation of 1509.9 m (WGS84 datum). The uncertainty in this position cannot be rigorously computed and is best expressed as a probability density function since it is dominated by systematic errors based on the following considerations. In R.A. the position ranges from  $-185$  to  $+342 \mu\text{as}$  ( $-0.3$  to  $+0.6$  km) from the reported position. The decl. ranges from  $-2.8$  to  $+0.2$  mas ( $-5.2$  to  $0.4$  km). Within these ranges, the distribution is nearly uniform. The position angle of the major axis of this distribution is  $3.6^\circ$  east of north due to the projected motion of Justitia relative to the star. This distribution is described by both Gaussian and uniform variants in the down-track and cross-track directions. The down-track errors are essentially zero, the systematic component was set to zero, and the Gaussian component is  $0.44$  km divided by  $\sqrt{19}$  for the number of chords and a formal value is less than  $1$  m. The cross-track errors were modeled with a Gaussian component of  $\sigma = 0.1$  km and a uniform distribution from  $-1$  to  $+5$  km.

The star  $(\alpha, \delta)$  position from DR3 is uncertain by  $(161, 93) \mu\text{as}$ . This star position uncertainty includes only the random components and is given for rough guidance only. When using this position, a full treatment of the uncertainties in the Gaia data should be used. The positions above are based on DR3 but can easily be revised when a newer and better catalog becomes available. When combined with the occultation result, the dominant uncertainty in decl. is from the occultation measurement. In R.A., both the star and the occultation contribute. The Gaussian components from the occultation are completely overwhelmed by the star catalog uncertainty. Using just the star uncertainties as an approximation is within a factor of 2 of the fully propagated value.

The uncertainty in the center of the hull is essentially all in the cross-track direction. The constraint in the down-track direction is extremely small. Our assumption that the center of the body corresponds to the position of the center of mass is likely prone to more error than the formal measurement down-track.

The cross-track position could be affected by a systematic error due to the relatively poorer constraint of the limb at the bottom of the figure. The maximum error would be a northward shift of the edge by  $5$  km. The center shift would be about  $150$  m, corresponding to a  $80 \mu\text{as}$  shift which is slightly less than the decl. uncertainty in the position of the star. However, this error estimate is a maximum reasonable error, not a Gaussian uncertainty. A more appropriate model for the uncertainty of the hull center is a one-sided uniform distribution that ranges from zero northward to  $80 \mu\text{as}$  along a line perpendicular to the shadow track. With a DR3 position, this level of detail in the uncertainty of the position is not needed and simple approximations will suffice.

## 6. Discussion

The shape provided by the occultation is poorly represented by an ellipse and complicates quantifying the albedo and its uncertainty. The total area from the occultation is  $2626 \text{ km}^2$  from our adopted limb profile. The lower bound on the area is  $2557 \text{ km}^2$ , but requires more peculiar topography. Using these values, the circular equivalent diameters are  $57.8$  and  $57.0$  km, but we prefer the larger value because it is smoother. Deriving an albedo requires an absolute magnitude. The value derived from the Minor Planet Center data is  $H_V = 9.74$ , but this measurement often contains systematic errors. The absolute magnitude is also available from the Fink Portal, described in B. Carry et al. (2024). From that site,  $H_g = 10.41 \pm 0.13$  and  $H_r = 9.56 \pm 0.13$  using the SHG1G2 model. The Zwicky Transient Facility (ZTF) data supporting this measurement do well at constraining the larger phase-angle photometric behavior, but there are limited data below  $3^\circ$  and the phase coefficients are uncertain for the opposition surge determination. Also, the portal does not correct for the rotational lightcurve, thus inflating the uncertainties of final derived absolute magnitudes. At the moment, this is the best available source and will be used for the albedo determination. Transforming the ZTF photometry to a standard  $V$  magnitude provides  $H_V = 9.82$ .

Before deriving an albedo, the mean absolute magnitude needs to be corrected for rotation. We have separate data taken, using a Johnson  $V$  filter, near the time of the occultation to facilitate this correction. Those data are not yet absolutely calibrated, but the shape of the lightcurve from data taken between 2023 October 1 and 2023 October 30, inclusive, is shown in Figure 6. The mean magnitude (horizontal line) is set to the Fink/ZTF value. The lightcurve of Justitia is quite complex but the occultation happened very near the lightcurve maximum. The vertical dashed line is the rotational phase at the time of the pre-event calibration measurements of Justitia relative to the star. The solid vertical line is at the time of the occultation. The difference between these two closely spaced epochs is quite small, well below the uncertainties in the absolute magnitude itself. Our final adopted absolute magnitude is  $H_V = 9.7 \pm 0.1$ . Once a better absolute magnitude can be determined, the albedo can be corrected accordingly. The nominal values yield a geometric albedo of  $p_V = 0.072$ . The  $0.1$  mag uncertainty on  $H_V$  would change the albedo by  $0.007$ . The lower bound to the area would add an additional shift of  $0.002$ . This uncertainty on the albedo is not a formal Gaussian uncertainty but chosen to match the uncertainty in the absolute magnitude. Eliminating this uncertainty could improve the albedo determination, limited only by the tight limits on the area.

The surface-equivalent sphere diameter from the radiometric CITPM solution was  $58 \pm 2$  km (A. Marciniak et al. 2025) with

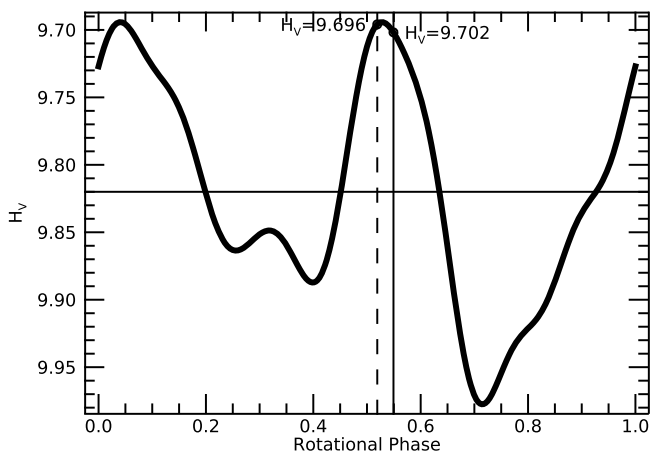


**Figure 6.** Lightcurve correction from the mean to the time of occultation. This is a smooth curve representation of the Justitia lightcurve within a month of the occultation. The horizontal line is the mean of the displayed lightcurve set to the Fink/ZTF value. The dashed line shows the rotational phase during the pre-event calibration photometry. The solid vertical line marks the rotational phase at the time of the occultation.

an albedo of  $0.058 \pm 0.006$ . Both parameters are in reasonably good agreement with each other, though the thermal modeling does seem to produce a slightly lower albedo different enough to require pushing all of the uncertainties favorably to produce agreement. At this point, the absolute magnitude needs the most attention to resolve this minor difference.

These data are insufficient to place quantitative limits on secondary bodies in orbit around Justitia. The observed offset from the ephemeris can be absorbed entirely by a refit of the orbit while including the occultation data. It will take at least two more occultation campaigns of similar quality to establish meaningful limits on secondary bodies through constraints on barycentric offsets from the orbit. Clearly the orbit quality is already quite good and poses no particular challenge with regard to future occultation efforts.

The coarse and fine detail in the limb profile clearly shows an irregularly shaped object. Justitia is large enough that a general expectation of a smoother shape is often encountered. From these data it is clear that an elliptical or spheroidal approximation to the size and shape hides a lot of important detail about Justitia. For instance, the projected polar axis is nearly vertical (i.e., north) at this time. The minor axis of the ellipse would generally be expected to align with the spin axis. In this case, the irregular shape leads to an inference of the axial orientation from an ellipse that is quite different from the guiding axes from the limb fit.

There are three regions that present a nearly straight edge in this projection: points 16–25 spanning 23 km, 27–32 spanning 38 km, and 40–7 spanning 26 km. The bottom of the object could also be another flat region. The curve shown here is the least flat plausible profile between points 7 and 9. Most of the limb structure is fairly smooth, but points 0–2 and 12 indicate some topographical signatures on a scale at or below a few kilometers.

## 7. Conclusions

These data are the first multi-chord occultation measurement of Justitia. No special effort was required for the prediction, only an interest in learning more about the object. Results like this are now possible for essentially all known solar system objects given suitable occultation opportunities (see M. W. Buie et al. 2020; B. Sicardy et al. 2024). Main-belt

asteroids provide the easiest of all such bodies given the current state of star positional catalogs and the asteroid orbit catalog. Due to the proximity of this event to a large amount of mobile equipment and interested people, the deployment was relatively inexpensive to support. Most of the observers contributed their time and effort for training, practice, and observing at no cost to the project. Even so, our collective ability to use occultations to study the small-body population in the solar system is limited by the amount of support available.

Justitia is confirmed to have a low albedo, and with that a well constrained absolute size. Exactly how low the albedo is remains a work in progress awaiting better determination of Justitia's absolute magnitude. The diameter of an equivalent-volume sphere is 57.0–57.8 km (consistent with the equivalent diameter of Justitia from the thermophysical model by A. Marciniak et al. 2025). Additional observations will provide further refinements to the three-dimensional shape of the body and refute, constrain, or detect the existence of a secondary mass.

This result shows the clear advantages provided by including detailed occultation limb profiles along with all of the other types of data routinely collected on small bodies, especially lightcurve and thermal emission data. By combining all three of these types of data, we have a much more secure determination of the basic physical properties. In particular, adding occultation data eliminates a large source of systematic error in the determination of the polar axis of a small body.

## Acknowledgments

Funding of the Emirates Mission to the Asteroid Belt is provided by the UAE Space Agency and helped support this research.

Thanks to all our other essential contributors for the observing campaigns: Safa Al Hosani, Fahad Albaeek (حور المازمي), Sultan Alblooshi, Fatema Alhameli (فاطمة سعيد الهاملي), Mariam Alharmoudi, Hamdan Almansoori, Salama AlMazrouei, Khaled Alnaqbi, Moza AlSerkal, W. Hunter Daboll, Sean Fitze, Brian Kirby, Elizabeth G. Kirby, Reem Klaib (كليب ريم), Daniel Kubitschek, Tom Masterson, Terry Miller, Christopher O'Neill, Anna Sophia Rorrer Warren, and João Vaz Carneiro.

The work of A.M. was supported by the National Science Centre, Poland, through grant No. 2020/39/O/ST9/00713.

## ORCID iDs

Marc W. Buie <https://orcid.org/0000-0003-0854-745X>

Hoor AlMazmi (حور المازمي) <https://orcid.org/0000-0002-0996-8857>

Paul Hayne <https://orcid.org/0000-0003-4399-0449>

Anna Marciniak <https://orcid.org/0000-0002-1627-9611>

Brian A. Keeney <https://orcid.org/0000-0003-0797-5313>

Noora Rashed Alsaeed <https://orcid.org/0000-0001-6622-4128>

Arvind Jayashankara Aradhya <https://orcid.org/0000-0002-8995-2408>

Dahlia Baker <https://orcid.org/0009-0001-0141-4016>


Samuel F. A. Cartwright <https://orcid.org/0000-0002-2751-3573>

Hugh M. Davidson <https://orcid.org/0009-0004-5447-2801>

Chelsea Ferrell <https://orcid.org/0000-0002-2530-0427>

Kai Getrost <https://orcid.org/0009-0005-7316-6671>

Julian Hammerl <https://orcid.org/0000-0003-1296-7203>

Parker Hinton  <https://orcid.org/0000-0001-9504-0520>  
 Jack L. Jewell  <https://orcid.org/0000-0001-8991-2599>  
 John Keller  <https://orcid.org/0000-0002-0915-4861>  
 Vadim Nikitin  <https://orcid.org/0009-0007-7900-4811>  
 Heshani Pieris  <https://orcid.org/0009-0005-1039-1548>  
 Arunima Prakash  <https://orcid.org/0000-0003-0793-5266>  
 Julien Salmon  <https://orcid.org/0000-0002-5977-3724>  
 Michael Skrutskie  <https://orcid.org/0000-0001-8671-5901>  
 Kya C. Sorli  <https://orcid.org/0009-0009-0386-6241>  
 Anne J. Verbiscer  <https://orcid.org/0000-0002-3323-9304>

## References

- AlMazmi, H. A., Hayne, P. O., Alsaeed, N., et al. 2024, in Int. Astronautical Congress, IAC-24-A3.4.B3
- Buie, M. W., Keeney, B. A., Strauss, R. H., et al. 2021, *PSJ*, **2**, 202
- Buie, M. W., & Keller, J. M. 2016, *AJ*, **151**, 73
- Buie, M. W., Porter, S. B., Tamblyn, P., et al. 2020, *AJ*, **159**, 130
- Bus, S. J., & Binzel, R. P. 2002, *Icar*, **158**, 106
- Carry, B., Peloton, J., Le Montagner, R., Mahlke, M., & Berthier, J. 2024, *A&A*, **687**, A38
- Đurech, J., Delbo', M., Carry, B., Hanuš, J., & Ali-Lagoa, V. 2017, *A&A*, **604**, A27
- Gaia Collaboration, Brown, A. G. A., Vallenari, A., et al. 2021, *A&A*, **649**, A1
- Hasegawa, S., Marsset, M., DeMeo, F. E., et al. 2021, *ApJL*, **916**, L6
- Humes, O. A., Thomas, C. A., & McGraw, L. E. 2024, *PSJ*, **5**, 80
- Mahlke, M., Carry, B., & Mattei, P. A. 2022, *A&A*, **665**, A26
- Mainzer, A. K., Bauer, J. M., Cutri, R. M., et al. 2019, NASA Planetary Data System, urn:nasa:pds:neowise\_diameters\_albedos::2.0, doi:10.26033/18S3-2Z54
- Marciniak, A., Ali-Lagoa, V., Müller, T. G., et al. 2019, *A&A*, **625**, A139
- Marciniak, A., Choukroun, A., & Perla, J. 2025, *PSJ*, **6**, 60
- Masiero, J. R., Mainzer, A. K., Bauer, J. M., et al. 2020, *PSJ*, **1**, 5
- Masiero, J. R., Mainzer, A. K., Grav, T., et al. 2012, *ApJL*, **759**, L8
- Sicardy, B., Braga-Ribas, F., Buie, M. W., Ortiz, J. L., & Roques, F. 2024, *ARA&A*, **32**, 6